



Chinese Society of Aeronautics and Astronautics
& Beihang University

Chinese Journal of Aeronautics

cja@buaa.edu.cn
www.sciencedirect.com



Oblique detonation wave triggered by a double wedge in hypersonic flow

Honghui TENG^a, Yuhang ZHANG^a, Pengfei YANG^{b,c,*}, Zonglin JIANG^{b,c}

^a School of Aerospace Engineering, Beijing Institute of Technology, Beijing 100081, China

^b State Key Laboratory of High Temperature Gas Dynamics, Institute of Mechanics, Chinese Academy of Sciences, Beijing 100190, China

^c School of Engineering Sciences, University of Chinese Academy of Sciences, Beijing 100049, China

Received 16 November 2020; revised 11 December 2020; accepted 5 February 2021

Available online 21 October 2021

KEYWORDS

Double wedge;
Hypersonic flow;
Initiation structures;
Oblique detonation;
Shock interactions

Abstract Pressure-gain combustion has gained attention for airbreathing ramjet engine applications owing to its better thermodynamic efficiency and fuel consumption rate. In contrast with traditional detonation induced by a single wedge, the present study considers oblique shock interactions attached to double wedges in a hypersonic combustible flow. The temperature/pressure increases sharply across the interaction zone that initiates an exothermic reaction, finally resulting in an Oblique Detonation Wave (ODW). Compared with the case for a single-wedge ODW, the double-wedge geometry has great potential to control the initiation of the ODW. As a tentative study, two-dimensional compressible Euler equations with a two-step induction-reaction kinetic model are used to solve the detonation dynamics triggered by a double wedge. The effects of the wedge angles and wedge corner locations on the initiation structures are investigated numerically. The results show an ODW complex comprising three Oblique Shock Waves (OSWs), an induction zone, a curved detonation front, and an unburned/low-temperature gas belt close to the surface of the second wedge. Both the increasing wedge angle and downstream wedge corner location lead to an abrupt OSW–ODW transition type, whereas the former corresponds to the shock–shock interaction and the later has a greater effect on the exothermic chemical process. Analysis of the shock polar and flow scale confirms that the OSW–ODW initiation structure mainly depends on the coupling of shocks and heat release in a confined initiation zone.

© 2021 Chinese Society of Aeronautics and Astronautics. Production and hosting by Elsevier Ltd. This is an open access article under the CC BY-NC-ND license (<http://creativecommons.org/licenses/by-nc-nd/4.0/>).

* Corresponding author at: State Key Laboratory of High Temperature Gas Dynamics, Institute of Mechanics, Chinese Academy of Sciences, Beijing 100190, China.

E-mail address: young1505@foxmail.com (P. YANG).

Peer review under responsibility of Editorial Committee of CJA.



Production and hosting by Elsevier

1. Introduction

Gaseous detonation is a type of supersonic combustion phenomenon across which temperature and pressure increase sharply. Owing to their high power density, pressure gain combustion systems based on detonations have received increasing attention.^{1–5} When the inflow velocity is higher than the Chapman–Jouguet (CJ) velocity, an oblique detonation wave can be

triggered by a wedge in a hypersonic combustible flow. The standing Oblique Detonation Wave (ODW) is suitable for combustion in a hypersonic flow, particularly as an alternative to the Oblique Detonation Engine (ODE)^{6,7} and Ram Accelerator (RA).⁸ Although some empirical models of the wave configuration have been proposed, the initiation structure of ODW is sensitive to gas-dynamic parameters and chemical parameters. To employ the ODW, it is critical to understand the shock and heat release coupling in supersonic inflow. Furthermore, only by adjusting the mechanical components, detonation engine achieves stable combustion in a wide range of inflow parameters.

Early works^{9–11} assumed that the chemical reaction was instantaneous and the flow was uniform; i.e., the heat release layer is infinitely thin and there a fixed oblique detonation angle for a given deflection angle. The stabilizations, wave angles, and thermodynamic states were analyzed using the shock/detonation polar. The coupling of shock and heat release generates a finite exothermic layer and initiation zone. The former is critical to cellular structures while the latter inspired many studies on the control and formation of the initiation zone. Wedge-induced ODW structures have been presented in many previous studies^{12,13}, showing that the initiation zone is a combination of shocks, deflagrations, and detonations. Moreover, a stable delayed ODW has been observed experimentally in hydrogen–air stoichiometric mixtures¹⁴ and the co-existence of an initiation zone has been confirmed. Thereafter, there have been extensive investigations on the wave structure near the initiation zone and the stability of detonation surface. The former aspects focused on the wave morphologies of ODW initiation^{15–25}. The latter work mainly analyzed the formation and evolution processes of ODW cellular structures.^{26–30} Recently, a panoptic review of ODWs is presented by Teng and Jiang.³¹ The review contains broad discussions on multi-wave structure and surface stability of oblique detonations under ideal/inhomogeneous inflow conditions. Derived from the practical application in ODEs, the operation of combustor involves the mixtures,^{21,32} inflow parameters,³³ unsteady processes³⁴ and confined spaces.^{35–37} The related research progress of the above aspects were also summarized and commented.³⁸ However, there are still outstanding issues and questions to be answered. The ODWs triggered by a finite-length wedge or cone have been simulated to explore more complicated but more realistic wave structures and dynamics. As an example, unstable ODWs were observed with periodic oscillation of the initiation zone or downstream surface.^{39,40} The interaction of the expansion wave and ODW in hydrogen–air mixtures demonstrates various wave dynamics near the quenching boundary.^{41,42} To facilitate the performance of propulsion, the expansion wave is also used to realize a near-CJ ODW.⁴³ The hot jet flow has been used to induce an ODW for a shorter initiation length.⁴⁴ Additionally, the lower limit of standing window of ODW is also modified by considering the pathological detonation feature.⁴⁵

The simplified ODE geometry is illustrated in Fig. 1(a), in which the ODW is induced by a double wedge. The zoomed computational domain in Fig. 1(b) was used to simulate the effects of Shock-Shock Interaction (SSI) on the ODW initiation structures. It should be noted that the diffusion effects may introduce some differences on wave morphologies. Yu and Miao⁴⁶ analyzed the effects of the turbulence intensity on the wedge-induced ODW initiation features, and found that

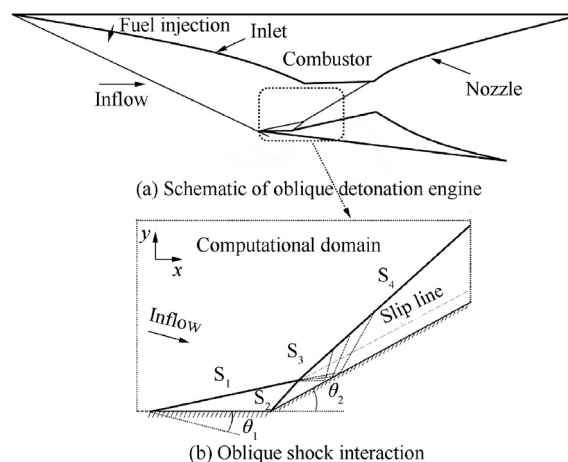


Fig. 1 Schematic of oblique detonation engine and an oblique shock interaction induced by a double wedge in supersonic flow.

initiation structures will change from abrupt transition to smooth one under the strongly turbulent flow. The incoming boundary layer is also considered in previous study.⁴⁷ The result shows that the shock-boundary layer interaction may lead to some separation bubbles. Notably, for the smooth ODW initiation structure, if the boundary layer is thin enough, the ODW structures are pretty same between viscous and inviscid flows.

From the viewpoint of shock and heat release coupling, the finite-length wedge introduces a shock-expansion wave configuration, which triggers a heat release in supersonic combustible inflow. Although the SSI configurations have been studied widely in the field of aerodynamics,^{48–52} the performance of the shock interactions in combustible inflow has not been addressed. As shown in Fig. 1(b), a triple-shock wave configuration is usually formed by a double wedge in hypersonic inflow, and this is referred to as a Type VI shock interaction.⁵³ In reacting flow, the initiation length of ODWs is sensitive to inflow conditions, which introduces challenges to the application of the ODW in an engine combustor. For the double wedge geometry, the first small wedge suppresses upstream movement of the detached ODW and the second large wedge contributes the initiation of the ODW under a low inflow Mach number. The present complicated shocks might be advantageous to detonation initiation and wave regulation, and thus possibly be employed in the ODE and RA. Therefore, ODWs triggered by the Type VI SSI are simulated and analyzed in this paper, clarifying flow features from the viewpoints of the detonation initiation and SSI.

2. Physical and mathematical models

To facilitate simulation, the coordinate frame is aligned in the direction along the first wedge surface. Following many previous studies,^{12,32–37,40–42,54} the reactive Euler equations are used as governing equations for modeling the ODW flow field. To implement the two-step chemical reaction model for chain-branching kinetics,⁵⁵ two additional reaction indexes are introduced: the induction reaction index ξ and the heat release index η . The chemical rate equations are given by:

$$\dot{\omega}_1 = H(1 - \xi)\rho k_I \exp\left[E_I\left(\frac{1}{T_S} - \frac{1}{T}\right)\right] \quad (1)$$

$$\dot{\omega}_2 = [1 - H(1 - \xi)]\rho(1 - \eta)k_R \exp\left(-\frac{E_R}{T}\right) \quad (2)$$

with the Heaviside step function:

$$H(1 - \xi) = \begin{cases} 1 & \xi \leq 1 \\ 0 & \xi > 1 \end{cases} \quad (3)$$

The specific total energy is thus expressed as:

$$e = \frac{p}{\rho(\gamma - 1)} + \frac{1}{2}(u^2 + v^2) - \eta Q \quad (4)$$

where $\dot{\omega}_1$ and $\dot{\omega}_2$ represent the reaction rate of the induction zone and heat release zone, respectively. The variables ρ , u , v , p , e , γ and Q are respectively the density, x -direction velocity, y -direction velocity, pressure, specific total energy, specific heat ratio and amount of chemical heat release. T is the gas temperature and T_S is the post-shock temperature of the one-dimensional CJ detonation. The energy release amount Q and activation energies (E_I and E_R) have been scaled with RT_0 . R is the gas constant and T_0 is the inflow gas temperature. Consistent with previous studies,^{28,54,55} two rate constants, k_I and k_R , are necessary to complete this chemical model: k_R is fixed to 1.0 and $k_I = -u_{vn}$, where u_{vn} is the particle velocity behind the shock front in the shock-fixed frame for a CJ detonation, whereby the induction length of the one-dimensional CJ detonation is fixed to unity. Hence, the reference scale l_{ref} is the induction length of a CJ detonation. The reference time scale t_{ref} is therefore set to be the value l_{ref}/c and $c^2 = RT_0$. All the variables have been non-dimensionalized by reference to the inflow state (the symbol “ \sim ” denotes original dimensional quantities and subscript “0” indicates reference quantities ahead of the detonation/shock front):

$$\rho = \frac{\tilde{\rho}}{\rho_0}, p = \frac{\tilde{p}}{p_0}, T = \frac{\tilde{T}}{T_0}, u = \frac{\tilde{u}}{\sqrt{RT_0}} \quad (5)$$

The governing equations are solved using the AUSM-type (Advection Upstream Splitting Method) splitting with a third-order MUSCL (Monotone Upstream-centered Schemes for Conservation Laws) approach. To achieve sufficient resolution for the simulations, the third-order Runge–Kutta algorithm is chosen as the time-discretization scheme. AUSMPW+ is designed to improve on the accuracy and efficiency of its predecessors through the introduction of a new numerical speed of sound and simplification of AUSMPW (AUSM by pressure-based weight functions). AUSMPW+ has higher resolution in capturing oblique shocks than any other AUSM-type scheme and eliminates the unphysical expansion shocks. Furthermore, AUSMPW+ scheme is more efficient to implement than AUSMPW while maintaining the same levels of robustness and accuracy.⁵⁶ As shown in Fig. 1(b), the computational domain is enclosed by the dot line and the wedge surface. Slip boundary condition is used on the wedge surface, which starts from $x = 0$ on the lower boundary. The left and upper boundaries are modeled as inflow boundary conditions, in which the inflow parameters are fixed to be constant. Outflow conditions extrapolated from the interior are implemented on the right and lower boundaries before the wedge due to the supersonic

flow. Besides, the inflow Mach number Ma_0 is fixed at 7.0 and the wedge angles θ_1 and θ_2 are varied to get different structural configurations of the ODW.

By reference to previous studies,^{47,57} the viscosity effects are mainly derived from the interaction between boundary layer and strong shock waves. The resulting separation bubble is a key factor to determine the initiation structures of ODW. As shown in Fig. 1(a), the coming boundary layer of a combustor is mainly derived from the upper inlet wall. The incoming boundary layer of the lower wall is no necessity to take into consideration. Actually, many studies^{36,37} have estimate the vicious effects in high-speed flow and demonstrate that the vicious effects can be neglected partly.

For the cases simulated in this study, the chemical parameters are set as $Q = 25$, $\gamma = 1.2$, $E_I = 4.0 T_S$, and $E_R = 1.0 T_S$. The parameters do not correspond to any realistic reactants but rather a generic model with modest heat release and activation energies. The propagation Mach number of one-dimensional CJ detonation is 4.5, which is about equal to the CJ velocity of the stoichiometric hydrogen-air mixture (100 kPa and 300 K). By referring to the induction length of the hydrogen-air mixture, we can estimate roughly that the computational domain may reach several centimeters. It is difficultly to induce a separation bubble on the wedge surface. Hence, we keep using Euler equations in this study for the negligible incoming boundary layer and thin boundary layer on wedge surface. As a preliminary study of ODWs induced by double wedge, we mainly focus the initiation structures and investigate the feasibility of double wedge ODW.

3. Results and discussion

3.1. Basic structures and resolution study

In this section, we present the basic structures of ODWs induced by the double wedge geometry and the independence of the flow features with respect to the grid scale. The numerical cases in this work are carefully chosen to avoid heat release on the first wedge surface. Otherwise, the second wedge may compress the combustion product and there is a loss of total pressure. This is unacceptable for a high-speed propulsion system. Fig. 2 shows the numerical temperature and pressure fields for wedge angles of $\theta_1 = 15^\circ$ and $\theta_2 = 15^\circ$. Similar to the case under the purely supersonic flow (see Fig. 1), the first attached oblique shock (S_1) from the nose intersects the attached shock (S_2) derived from the corner of the wedge. The contact surface separates the flow that has passed through both oblique shocks from the flow that passed only through the oblique shock (S_3). A Prandtl–Meyer expansion fan is emitted from the intersection point and reflects from the surface of the second wedge. Considering the chemical reaction, there is a shock-reaction complex. A curved ODW forms downstream owing to the high temperature behind the interaction zone. Compared with the case for the single wedge ODW,⁵⁴ there is an unburned/low-temperature gas belt close to the surface of the second wedge. The initiation structures above the gas belt are similar to those of the single-wedge ODWs. Overall, the wave complex of the double wedge ODW consists of three oblique shocks, an initiation zone, a cured detonation, and an unburned/low-temperature gas belt close to the surface of the second wedge.

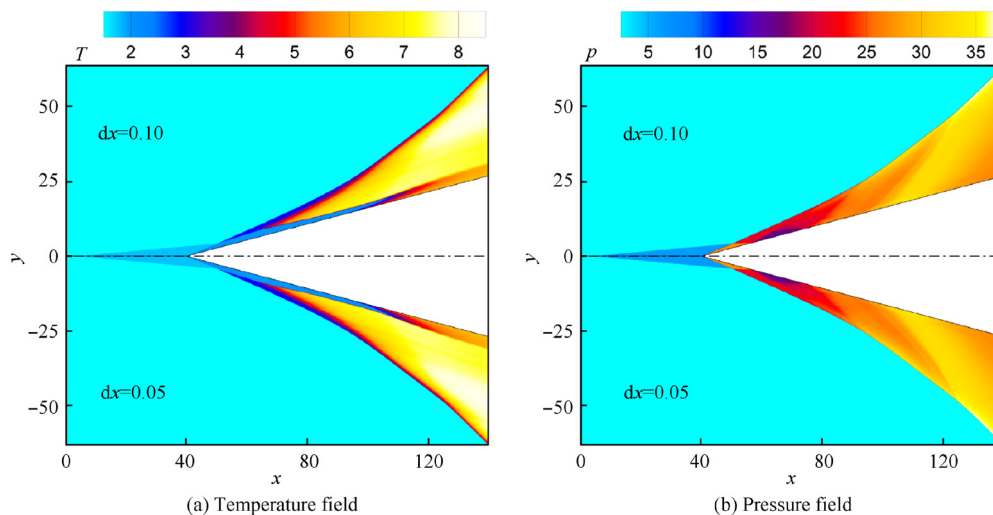


Fig. 2 Temperature and pressure fields obtained for different grids with wedge angles of $\theta_1 = 15^\circ$ and $\theta_2 = 15^\circ$.

To verify grid convergence, the flow fields of the ODW obtained using the finer scale $dx = 0.05$ are also shown in Fig. 2. The general wave structures are essentially the same except for a slight difference in the product pressure contours. For a further quantitative comparison, the temperature/pressure profiles along the wedge surface and the line $y = 30$, parallel to the x -axis, are shown in Fig. 3. The thermodynamic parameters have two growth peaks owing to the corner of the double wedge, as shown in Fig. 3(a). Then, the pressure drops rapidly and the temperature decreases slightly owing to the emission of expansion waves from the intersection point. A slow increase in pressure results from the contraction of the unburned gas belt that is squeezed by the heat release of the flow across the oblique shock S_3 . At the downstream shock surface, the pressure and temperature rapidly increase synchronously owing to the strong coupling of the shock front and heat release zone. Results show that curves overlap each other and differences are hardly distinguishable. The default mean scale (i.e., $dx = 0.1$) is shown to provide well-converging initiation structures, sufficient to guarantee the reliability of the conclusion, and this scale is thus used subsequently in the present work.

3.2. Effects of secondary wedge angle

In the case of the double wedge geometry, the wedge angles and wedge corner locations are crucial to the initiation structures of the ODW. A different type of interaction occurs as the secondary wedge angle θ_2 increases in supersonic nonreactive flow, and thus types have been identified.⁵³ For the shock complex induced by double wedge under nonreactive flow, there exists a critical angle $\theta_{2,cr}$ which can dominate the interaction types. When the first wedge angle equals to 15° , the critical angle $\theta_{2,cr}$ is 38.1° for the inflow parameters $Ma_0 = 7.0$ and $\gamma = 1.2$. Below the critical angle $\theta_{2,cr}$, a Type VI interaction occurs, as shown in Fig. 1(b). Conversely, if the second wedge angle is greater than $\theta_{2,cr}$, the interaction type will change from Type VI interaction to Type V one.^{49,53} Note that, the chosen wedge angle is far less than the critical angle $\theta_{2,cr}$ in this study, hence the SSI type will maintain the Type VI interaction. Considering the heat release behind the interaction zone and that the Arrhenius form of the chemical reaction rate is sensitive to temperature, a slight change in temperature may affect the ODW initiation structures. Fig. 4 shows the temperature fields of the ODW with the first wedge angles of

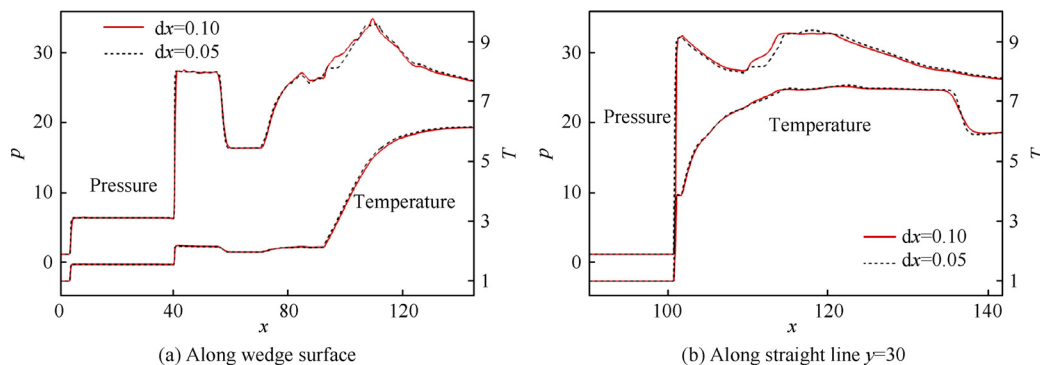


Fig. 3 Pressure and temperature along wedge surface and straight line $y = 30$ obtained for different grid sizes with wedge angles of $\theta_1 = 15^\circ$ and $\theta_2 = 15^\circ$.

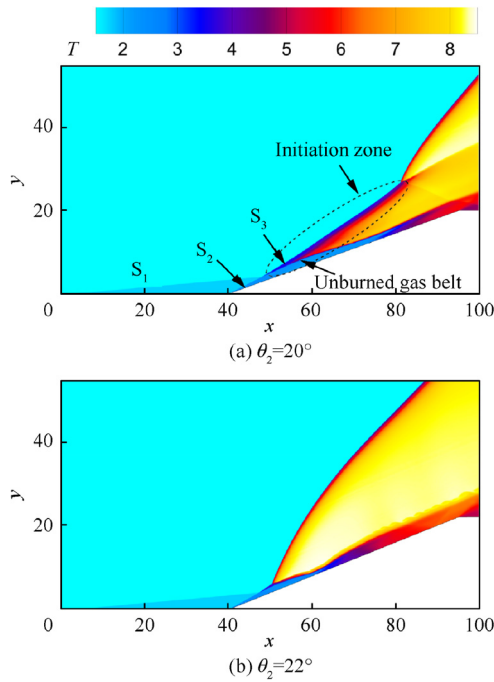


Fig. 4 Temperature fields with a first angle $\theta_1 = 15^\circ$ and second angles $\theta_2 = 20^\circ, 22^\circ$.

$\theta_1 = 15^\circ$. Note that basic structures, such as the straight oblique shocks, initiation zone, and unburned/low-temperature gas belt, still exist for the secondary wedge angles of $\theta_2 = 20^\circ, 22^\circ$. The main differences are the wave structures of the downstream ODW front. At an angle of $\theta_2 = 15^\circ$ (see Fig. 2), the OSW gradually transits to the curved ODW via the interaction between the pressure waves and chemical reaction front, which is described as a smooth transition. As θ_2 increases to 20° or 22° , there is a sudden shift on the downstream ODW surface. A multi-wave point appears and connects the initiation zone and the detonation front. Similar to what was observed in previous studies,^{15,16,18} the initiation structure shown in Fig. 4(a) is generally defined as an abrupt transition. A further increase in the angle θ_2 results in a bow-shaped detonation front and a decrease in the initiation length, as shown in Fig. 4(b).

For the ODW induced by a single wedge, detonation polar theory¹⁰ has demonstrated that there are two critical wedge angles, θ_{CJ} and θ_{detach} . For the wedge angle θ below a critical value θ_{CJ} , there is no real solution. If the wedge angle is greater than the detached value θ_{detach} , a strong solution occurs. In many previous studies,^{13,17,18,28} the chosen wedge angle is far less than θ_{detach} and greater than θ_{CJ} . They conclude that an increase in wedge angle promotes the formation of a smooth transition and the small wedge angle could lead to an abrupt transition. When the wedge angle is well close to the detached value, θ_{detach} , the strong solution may occur due to the interaction of complex waves in the induction zone. Hence, an abrupt transition arises at a large wedge angle.^{15,39,58} Similarly, when the second wedge angle increases, the abrupt transition of OSW-ODW is also observed in Figs. 2 and 4. More cases with different combinations of wedge angles are presented in Table 1. From the data, it can be seen that an increase in the second wedge angle could result in an abrupt transition.

Table 1 Transition patterns of ODWs with different combinations of wedge angles.

θ_1 ($^\circ$)	θ_2 ($^\circ$)	Type
5	25–32	Smooth
5	33	Abrupt
10	20–24	Smooth
10	25–27	Abrupt
15	15–17	Smooth
15	18–22	Abrupt
20	10–11	Smooth
20	12–17	Abrupt
25	5–8	Smooth
25	9–12	Abrupt

Compared to the results of single wedge ODW,^{15,39,58} it is concluded that the interaction of complex waves plays an important role in the formation of the ODW initiation structures.

Another point worth highlighting is the formation of the bow detonation front in Fig. 4(b), which shows an unsteady phenomenon in the early forming stages of the ODW, as shown in Fig. 5. For comparison purposes, the final steady shock front is plotted in each frame as a black solid line. In the initial stage of ODW evolution, as shown in Fig. 5(a), the wavefront structures can be divided into three parts, namely a non-reactive straight shock, curved shock, and curved detonation front. The overall flow structures are almost the same as those in Fig. 4(a), but the detonation front is unsteady. Fig. 5(b) and (c) shows that the wavefront is greatly raised and moves upstream. The shock wavefront fluctuates for several cycles until reaching the final steady location. A similar unsteady phenomenon was mentioned in a previous paper,⁵⁴ where the equilibrium state of the initiation wave structures was disturbed by the upstream detonation front and there were non-decaying oscillations of wave structures. Hence, the zone behind the reflected shock S_3 (see Fig. 1) is crucial to the formation and instability of the local initiation structures.

To discuss the effects of the interaction zone on the initiation structures quantitatively, the shock polar with an inflow Mach number $Ma_0 = 7.0$ is shown in Fig. 6. The symbol S_1 denotes the polar of the initial supersonic inflow; and the symbol S_2 corresponds to the flow that passed the first deflection angle. According to shock dynamics theory, the respective expansion polar can be computed as plotted in Fig. 6; this polar can be used to connect polar curves S_2 and S_3 . Blue, green, and magenta lines respectively represent expansion polar curves of secondary angles $\theta_2 = 15^\circ, 20^\circ, 22^\circ$. The intersection point of the shock polar and expansion polar denotes the pressure behind the shock. Hence, the black dots denote the thermodynamic state behind shock S_2 , showing that the pressure increases as the secondary wedge angle varies from 15° to 22° . Since the high pressure behind the shock S_2 , the expansion polar extends toward the bottom right and intersects the S_1 polar. These intersection points are marked by red dots that represent the pressure of the flow across the shock S_3 . Note that the pressure/temperature behind the reflected shock S_3 is equivalent to that induced by the single wedge (with angles of $32.7^\circ, 39.1^\circ, 41.6^\circ$) under the same inflow condition. For the single wedge having $Ma_0 = 7.0$ and $\gamma = 1.2$, the

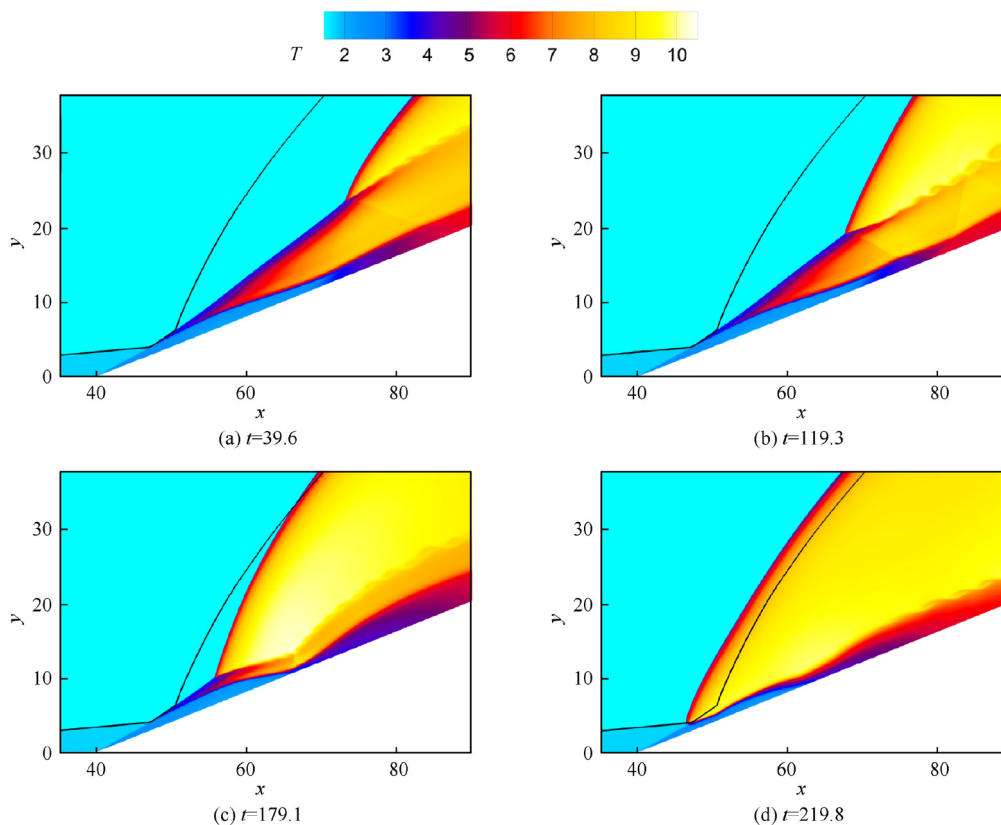


Fig. 5 Evolution of ODW initiation with wedge angles $\theta_1 = 15^\circ$ and $\theta_2 = 22^\circ$ (black line denotes final steady shock front).

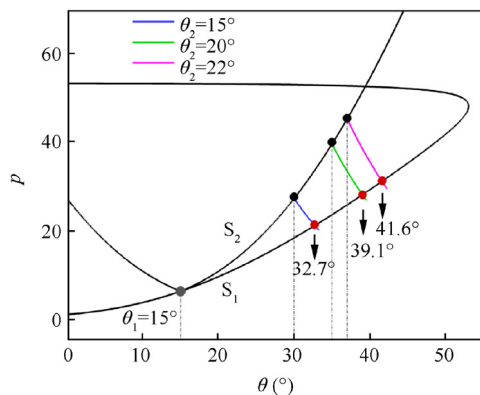


Fig. 6 Pressure polar of SSI for double wedge with the first wedge $\theta_1 = 15^\circ$.

theoretical detached angle of the ODW is 38.4° , beyond which the ODW detaches from the wedge surface. When the second wedge angle is 20° or 22° , the theoretical angle of reflected shock S_3 is 39.1° or 41.6° , respectively. Hence, the detonation front detaches locally, which could lead to an abrupt OSW–ODW transition.

As the second wedge angle increases, the pressure/temperature of the reactive flow across shock S_3 increases. The increasing post-shock temperature reduces the initiation length and shortens the distance between the ODW front and the interaction zone. From the viewpoint of chemical energy, the fast heat release promotes an abrupt OSW–ODW transition, which has

been demonstrated by adjusting the pre-exponential factor of the exothermic reaction.⁵⁴ The cited results are similar to the resulting initiation structures in the present work. However, many studies also demonstrated that a high inflow Mach number and large wedge angle are more inclined to result in a smooth transition, in which the post-shock temperature is higher.^{14,27,28} In other words, the post-shock temperature of the mixture is not the dominant parameter of OSW–ODW initiation structures. In addition to the thermodynamic parameter, the initiation of the detonation wave is also affected by the geometric size. For a supersonic combustible flow, time and space are required to complete the heat release process. The flow scale should be considered in the double wedge ODW.

3.3. Effects of wedge corner location

Many cases with different combinations of wedge angles (θ_1, θ_2) were simulated and three types of initiation structure are observed here. Fig. 7 shows the effects of the wedge corner location on the initiation structures. When the wedge corner is at $x = 20$, the OSW is connected to the downstream front via a smooth slender zone. In this zone, the main shock S_3 is enhanced via the pressure waves induced by heat release in supersonic flow, which contributes to detonation initiation. As the wedge corner moves downstream, the OSW–ODW transition type changes from the smooth one to the abrupt one. The appearance of the multi-wave point is critical to the ODW initiation types. A similar flow phenomenon, triggered by varying the wedge angles, was mentioned above. In the case

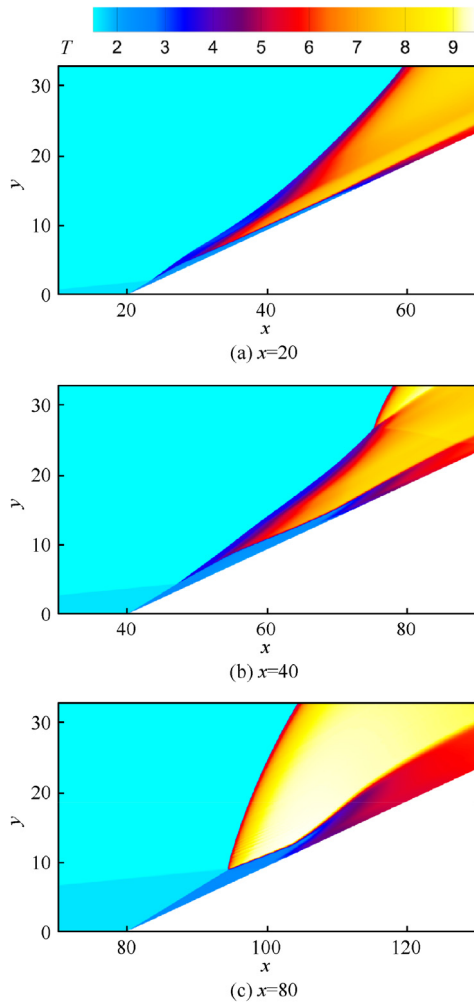


Fig. 7 Temperature fields with wedge angles $\theta_1 = 10^\circ$ and $\theta_2 = 25^\circ$, where location of wedge corner is set at $x = 20, 40, 80$.

of nonreactive supersonic flow, many previous studies^{48,49,53} showed that the interaction type is determined only by the inflow Mach number, specific heat ratio, and wedge angles. However, the chemical reaction is sensitive to temporal and spatial scales, and the geometry size can affect the exothermic process, as shown in Fig. 7. The downstream movement of the wedge corner results in a large SSI zone, in which the reflected shock S_3 has enough space and time to induce the heat release. More importantly, the reflected shock S_3 reduces the distance between the downstream ODW front and initiation zone. The fast heat release in this limited space preferentially leads to an abrupt OSW–ODW transition under some conditions.

For the differences in flow properties, the geometrical dimension may affect the release of the chemical energy. First, the OSW cases with wedge angles of $\theta_1 = 10^\circ$ and $\theta_2 = 25^\circ$ are simulated as shown in Fig. 8(a). The corresponding ODW cases are plotted in Fig. 8(b) for comparison. It is stressed that the spatial scale of OSW/ODW pressure contours with blue lines is zoomed out wholly. The original wedge corner location of flow fields with blue lines is at $x = 80$ (i.e., the pressure plotted by blue lines). For the nonreactive OSWs in Fig. 8(a), the pressure lines are almost overlapping, and there is only a little

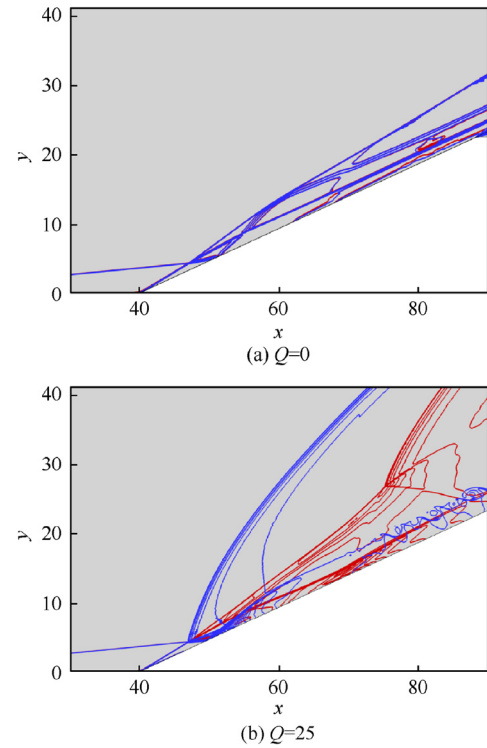


Fig. 8 Pressure contours of OSW/ODW with wedge angles $\theta_1 = 10^\circ$ and $\theta_2 = 25^\circ$, where chemical heat release is $Q = 0, 25$.

difference in the downstream fields near the wedge surface. Therefore, the flow structures of shock dynamics are self-similar; i.e., the geometric size is not a control parameter of flow features. However, the similarity law is not applicable to supersonic reactive flow. Fig. 8(b) shows a large difference in the scaling wave structure, especially in terms of the downstream detonation front. The OSW with red lines transforms into the detonation via a slender initiation zone involving complex interactions of compression waves and chemical reactions. In the case of the ODW with blue lines, the initiation zone is devoured by the bow detonation front. The geometric scale plays a key role in the initiation process of the ODW, since the heat release occurs.

On the whole, three types of ODW structures induced by the double wedge are observed, as shown in Fig. 9; i.e., smooth, abrupt I, and abrupt II types. Additionally, the initiation structures were generally found in many cases with different combinations of wedge angles (θ_1, θ_2) and wedge corner locations. The primary flow structures consists of three oblique shocks (S_1, S_2 and S_3), an expansion fan originating from the interaction point, an unburned/low-temperature gas belt, a curved detonation front, and reflected shocks. The main difference among of them is the final steady initiation structures. In this zone, shock waves induced by a wedge compress the flow and trigger a chemical reaction; in return, the heat release in the supersonic flow leads to a series of pressure waves that can enhance the flow pressure/temperature. The coupling of the curved shock and reaction front in a confined space can be treated as the dominant mechanism that determines the initiation structures and OSW–ODW transition type.

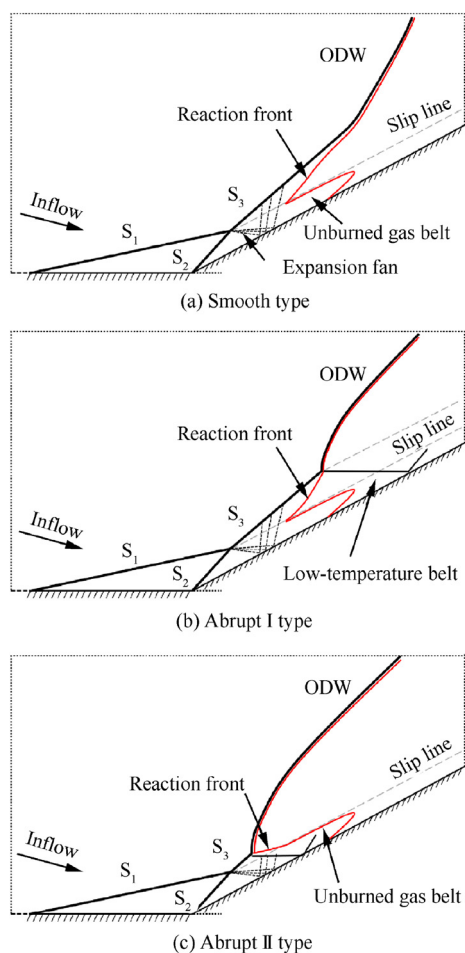


Fig. 9 Schematics of three basic initiation structures for ODW induced by double wedge.

4. Conclusions

ODWs triggered by a double wedge in hypersonic inflow were simulated to explore the basic initiation structures. The wave complex generally comprises an interaction zone involving three oblique shocks, an induction zone, an unburned/low-temperature gas belt, and a curved detonation front. Three types of the ODWs, namely a smooth type, abrupt I type, and abrupt II type, were observed in many cases.

- (1) For the single wedge ODW, an increase in the wedge angle leads to the appearance of a smooth initiation zone. Nevertheless, the OSW-ODW initiation structure changes from smooth to abrupt in the case of the double-wedge flow because of the SSI. Owing to the exothermic reaction behind the SSI zone, the similarity law for the pure shock configurations is not applicable to supersonic reactive flow. Subsequently, the varying location of the wedge corner affects the OSW-ODW initiation structure.
- (2) Moreover, the analysis of interactions among the shocks illustrates that the reflected oblique shock S_3 is crucial to the formation of the initiation structures, which could affect the transition type and the unsteadiness of the ODW front via the interaction of the compression waves

and heat release. The ODWs induced by double wedge contains several issues and the preliminary study mainly focused on the fundamental structures under the shock interactions.

- (3) By referring to previous studies,^{17,18} the increasing of inflow velocity and temperature will increase the post-shock temperature and reduce the initiation length, which benefits to the formation of a smooth transition. While the high pressure and activation energy are more likely to induce a sharp exothermic process and promote an abrupt transition.^{26,33} The supersonic flow and heat release interfere with each other. It is difficult to quantitatively analyze the formation of transition patterns. Considering the heat release process, some significant criterions have been proposed under detailed chemical models and realistic inflow conditions,^{25,33} which could deepen our understanding of initiation structures and help develop a practical airbreathing hypersonic propulsor.

Declaration of Competing Interest

The authors declare that they have no known competing financial interests or personal relationships that could have appeared to influence the work reported in this paper.

Acknowledgements

This study was supported by the National Natural Science Foundation of China (No. 11822202).

References

1. Kailasanath K. Recent developments in the research on pulse detonation engines. *AIAA J* 2003;**41**(2):145–59.
2. Wolański P. Detonative propulsion. *Proc Combust Inst* 2013;**34**(1):125–58.
3. Jiang ZL, Hu ZM, Wang YP, et al. Advances in critical technologies for hypersonic and high-enthalpy wind tunnel. *Chin J Aeronaut* 2020;**33**(12):3027–38.
4. Jiang ZL, Zhang ZJ, Liu YF, et al. Criteria for hypersonic airbreathing propulsion and its experimental verification. *Chin J Aeronaut* 2021;**34**(3):94–104.
5. Zhou R, Wu D, Wang JP. Progress of continuously rotating detonation engines. *Chin J Aeronaut* 2016;**29**(1):15–29.
6. Ashford SA, Emanuel G. Oblique detonation wave engine performance prediction. *J Propuls Power* 1996;**12**(2):322–7.
7. Sislian JP, Schirmer H, Dubeout R, et al. Propulsive performance of hypersonic oblique detonation wave and shock-induced combustion ramjets. *J Propuls Power* 2001;**17**(3):599–604.
8. Higgins AJ. Ram accelerators: Outstanding issues and new directions. *J Propuls Power* 2006;**22**(6):1170–87.
9. Gross RA. Oblique detonation waves. *AIAA J* 1963;**1**(5):1225–7.
10. Pratt DT, Humphrey JW, Glenn DE. Morphology of standing oblique detonation waves. *J Propuls Power* 1991;**7**(5):837–45.
11. Ghorbanian K, Sterling JD. Influence of formation processes on oblique detonation wave stabilization. *J Propuls Power* 1996;**12**(3):509–17.
12. Li CP, Kailasanath K, Oran ES. Detonation structures behind oblique shocks. *Phys Fluids* 1994;**6**(4):1600–11.
13. Vlasenko VV, Sabel'nikov VA. Numerical simulation of inviscid flows with hydrogen combustion behind shock waves and in detonation waves. *Combust Explos Shock Waves* 1995;**31**(3):376–89.

14. Viguier C, Figueira da Silva LF, Desbordes D, et al. Onset of oblique detonation waves: Comparison between experimental and numerical results for hydrogen-air mixtures. *Symp Int Combust* 1996;**26**(2):3023–31.
15. Papalexandris MV. A numerical study of wedge-induced detonations. *Combust Flame* 2000;**120**(4):526–38.
16. Figueira da Silva LF, Deshaies B. Stabilization of an oblique detonation wave by a wedge: a parametric numerical study. *Combust Flame* 2000;**121**(1–2):152–66.
17. Qin QY, Zhang XB. Study on the transition patterns of the oblique detonation wave with varying temperature of the hydrogen-air mixture. *Fuel* 2020;**274**: 117827.
18. Teng HH, Jiang ZL. On the transition pattern of the oblique detonation structure. *J Fluid Mech* 2012;**713**:659–69.
19. Miao SK, Zhou J, Liu SJ, et al. Formation mechanisms and characteristics of transition patterns in oblique detonations. *Acta Astronaut* 2018;**142**:121–9.
20. Miao SK, Zhou J, Lin ZY, et al. Numerical study on thermodynamic efficiency and stability of oblique detonation waves. *AIAA J* 2018;**56**(8):3112–22.
21. Zhang YH, Fang YS, Ng HD, et al. Numerical investigation on the initiation of oblique detonation waves in stoichiometric acetylene-oxygen mixtures with high argon dilution. *Combust Flame* 2019;**204**:391–6.
22. Gao Y, Li HY, Xiang GX, et al. Initiation characteristics of oblique detonation waves from a finite wedge under argon dilution. *Chin J Aeronaut* 2021;**34**(10):81–90.
23. Yang L, Yue LJ, Zhang QF, et al. Numerical study on the shock/combustion interaction of oblique detonation waves. *Aerosp Sci Technol* 2020;**104**: 105938.
24. Bian J, Zhou L, Teng HH. Structural and thermal analysis on oblique detonation influenced by different fore-body compressions in hydrogen-air mixtures. *Fuel* 2021;**286**: 119458.
25. Teng HH, Tian C, Zhang YN, et al. Morphology of oblique detonation waves in a stoichiometric hydrogen-air mixture. *J Fluid Mech* 2021;**913**:A1.
26. Choi JY, Kim DW, Jeung IS, et al. Cell-like structure of unstable oblique detonation wave from high-resolution numerical simulation. *Proc Combust Inst* 2007;**31**(2):2473–80.
27. Teng HH, Jiang ZL, Ng HD. Numerical study on unstable surfaces of oblique detonations. *J Fluid Mech* 2014;**744**:111–28.
28. Yang PF, Teng HH, Ng HD, et al. A numerical study on the instability of oblique detonation waves with a two-step induction-reaction kinetic model. *Proc Combust Inst* 2019;**37**(3):3537–44.
29. Zhang YN, Zhou L, Meng H, et al. Reconstructing cellular surface of gaseous detonation based on artificial neural network and proper orthogonal decomposition. *Combust Flame* 2020;**212**:156–64.
30. Martínez-Ruiz D, Huete C, Sánchez AL, et al. Theory of weakly exothermic oblique detonations. *AIAA J* 2019;**58**(1):236–42.
31. Teng HH, Jiang ZL. Progress in multi-wave structure and stability of oblique detonations. *Adv Mech* 2020;**50**(1) [Chinese] 202002.
32. Fang YS, Zhang YH, Deng X, et al. Structure of wedge-induced oblique detonation in acetylene-oxygen-argon mixtures. *Phys Fluids* 2019;**31**(2) 026108.
33. Tian C, Teng HH, Ng HD. Numerical investigation of oblique detonation structure in hydrogen-oxygen mixtures with Ar dilution. *Fuel* 2019;**252**:496–503.
34. Yang PF, Ng HD, Teng HH. Numerical study of wedge-induced oblique detonations in unsteady flow. *J Fluid Mech* 2019;**876**:264–87.
35. Zhang GQ, Li GX, Wang KL. Wave structure of oblique detonation disturbed by an expansion wave from a bended tunnel. *Appl Therm Eng* 2020;**180** :115856.
36. Wang KL, Zhang ZJ, Yang PF, et al. Numerical study on reflection of an oblique detonation wave on an outward turning wall. *Phys Fluids* 2020;**32**(4) :046101.
37. Wang KL, Teng HH, Yang PF, et al. Numerical investigation of flow structures resulting from the interaction between an oblique detonation wave and an upper expansion corner. *J Fluid Mech* 2020;**903**:A28.
38. Zhang YN, Yang PF, Teng HH, et al. Flow and combustion mechanism of oblique detonation engines. *Sci Sin-Phys Mech Astron* 2020;**50**(9) :090008[Chinese].
39. Choi JY, Shin EJR, Jeung IS. Unstable combustion induced by oblique shock waves at the non-attaching condition of the oblique detonation wave. *Proc Combust Inst* 2009;**32**(2):2387–96.
40. Liu Y, Han XD, Yao SB, et al. A numerical investigation of the prompt oblique detonation wave sustained by a finite-length wedge. *Shock Waves* 2016;**26**(6):729–39.
41. Fang YS, Hu ZM, Teng HH. Numerical investigation of oblique detonations induced by a finite wedge in a stoichiometric hydrogen-air mixture. *Fuel* 2018;**234**:502–7.
42. Xiang GX, Gao X, Tang WJ, et al. Numerical study on transition structures of oblique detonations with expansion wave from finite-length cowl. *Phys Fluids* 2020;**32**(5) :056108.
43. Bhatrai S, Tang H. Formation of near-Chapman-Jouguet oblique detonation wave over a dual-angle ramp. *Aerosp Sci Technol* 2017;**63**:1–8.
44. Li HB, Li JL, Xiong C, et al. Investigation of hot jet on active control of oblique detonation waves. *Chin J Aeronaut* 2020;**33**(3):861–9.
45. Xu Z, Dong G, Pan ZH, et al. Standing window of oblique detonation with pathological behaviour. *Chin J Aeronaut* 2021;**34**(5):496–503.
46. Yu MY, Miao SK. Initiation characteristics of wedge-induced oblique detonation waves in turbulence flows. *Acta Astronaut* 2018;**147**:195–204.
47. Miao SK, Xu DK, Song TL, et al. Shock wave-boundary layer interactions in wedge-induced oblique detonations. *Combust Sci Technol* 2020;**192**(12):2345–70.
48. Bertin JJ, Hinkle JC. Experimental investigation of supersonic flow past double-wedge configurations. *AIAA J* 1975;**13**(7):897–901.
49. Hu ZM, Myong RS, Kim MS, et al. Downstream flow condition effects on the RR → MR transition of asymmetric shock waves in steady flows. *J Fluid Mech* 2009;**620**:43–62.
50. Xue XP, Nishiyama Y, Nakamura Y, et al. High-speed unsteady flow past two-body configurations. *Chin J Aeronaut* 2018;**31**(1):54–64.
51. Xiang GX, Wang C, Teng HH, et al. Shock/shock interactions between bodies and wings. *Chin J Aeronaut* 2018;**31**(2):255–61.
52. Pasha AA, Juhany KA. Numerical simulation of compression corner flows at Mach number 9. *Chin J Aeronaut* 2020;**33**(6):1611–24.
53. Olejniczak J, Wright MJ, Candler GV. Numerical study of inviscid shock interactions on double-wedge geometries. *J Fluid Mech* 1997;**352**:1–25.
54. Yang PF, Teng HH, Jiang ZL, et al. Effects of inflow Mach number on oblique detonation initiation with a two-step induction-reaction kinetic model. *Combust Flame* 2018;**193**:246–56.
55. Ng H, Higgins A, Kiyanda C, et al. Nonlinear dynamics and chaos analysis of one-dimensional pulsating detonations. *Combust Theory Model* 2005;**9**(1):159–70.
56. Kim KH, Kim C, Rho OH. Methods for the accurate computations of hypersonic flows: I. AUSMPW+ Scheme. *J Comput Phys* 2001;**174**(1):38–80.
57. Li GX, Zhang GQ, Zhang YH, et al. Influence of viscous boundary layer on initiation zone structure of two-dimensional oblique detonation wave. *Aerosp Sci Technol* 2020;**104** :106019.
58. Morris CI. *Shock-induced combustion in high-speed wedge flows [dissertation]*. Stanford: Stanford University; 2001.